

1 High-field magnetoresistive effects in reduced-dimensionality organic metals and superconductors

J. Singleton, R.D. McDonald and N. Harrison.

National High Magnetic Field Laboratory, LANL, MS-E536, Los Alamos, New Mexico 87545, USA jsingleton@lanl.gov; rmcd@lanl.gov; nharrison@lanl.gov

Summary. The large charge-transfer anisotropy of quasi-one- and quasi-two-dimensional crystalline organic metals means that magnetoresistance is one of the most powerful tools for probing their bandstructure and interesting phase diagrams. Here we review various magnetoresistance phenomena that are of interest in the investigation of metallic, superconducting and charge-density-wave organic systems.

1.1 Introduction

Quasi-two-dimensional crystalline organic metals and superconductors are very flexible systems in the study of many-body effects and unusual mechanisms for superconductivity [1-7]. Their "soft" lattices enable one to use relatively low pressures to tune the same material through a variety of low-temperature groundstates, for example from Mott insulator via intermingled antiferromagnetic and superconducting states to unusual superconductor [4,6,7]. Pressure also provides a sensitive means of varying the electron-phonon and electron-electron interactions, allowing their influence on the superconducting groundstate to be mapped [3,4,8]. The self-organising tendencies of organic molecules means that organic metals and superconductors are often rather clean and well-ordered systems; as we shall see below, this enables the Fermi-surface topology to be measured in very great detail using modest magnetic fields [3,9]. Such information can then be used as input parameters for theoretical models [3]. And yet the same organic molecules can adopt a variety of configurations, leading to "glassy" structural transitions and mixed phases in otherwise very pure systems [4,10,11]; these states may be important precursors to the superconductivity in such cases [11].

Intriguingly, there seem to be at least two (or possibly three) distinct mechanisms for superconductivity [3,12-14] in the quasi-two-dimensional organic conductors. The first applies to half-filled-band layered charge-transfer salts, such as the BEDT-TTF and PbO packing arrangements of salts of the form $(\text{BEDT-TTF})_2\text{X}$, where X is an anion molecule; the superconductivity appears to be mediated by electron correlations/antiferromagnetic fluctuations [3,5]. The second mechanism applies to e.g. the PbO phase BEDT-TTF salts [4]; it appears to depend on the proximity of a metallic phase

to charge order [11][13]. Finally, there may be some instances of BCS-like phonon-mediated superconductivity [14].

The main purpose of this chapter is to discuss the role that high magnetic fields and magnetoresistance measurements, can play in unravelling the above-mentioned properties of quasi-one- and quasi-two-dimensional organic metals and superconductors. Hence, we shall spend some time discussing the high-field magnetotransport experiments that have helped to measure the Fermi surfaces of charge-transfer salts of molecules such as BEDT-TTF and BETS. In addition to their invaluable role in mapping the bandstructure, high magnetic fields allow one to tune some of the organic conductors into some new and intriguing phases; magnetoresistance phenomena can then be used to delineate the phase boundary of the new state. Examples include field-induced superconductivity [15] and exotic states such as the Fulde-Ferrell-Larkin-Ovchinnikov (FFLO) phase [16]. The phase diagram of the latter state in $-(\text{BEDT-TTF})_2\text{Cu}(\text{NCS})_2$ is shown in Fig. 1.1; its derivation is a good illustration of the general utility of high fields and magnetoresistive phenomena. First, a conventional (~ 30 Hz) measurement of the magnetoresistance was used to very precisely orient the sample in the magnetic field and to measure the superconducting-to-resistive transition [16]. Subsequently, high-frequency (MHz) magnetoresistance measurements that are sensitive to changes in dissipation within the zero-resistance state, allowed the FFLO to type II superconductivity boundary to be measured [16]. In view of recent doubts about the proposed FFLO state in CeCoIn_5 [17], organic conductors such as $-(\text{BEDT-TTF})_2\text{Cu}(\text{NCS})_2$ [16] and $-(\text{BETS})_2\text{GaCl}_4$ [18] are perhaps as yet the only systems in which the FFLO has been truly observed. Later in this paper, we shall describe other recent observations of field-induced phases in crystalline organic metals, which are related to the FFLO but which result in insulating states.

The remainder of this chapter is organized as follows. Section 1.2 describes the Fermi-surface topologies of some typical organic charge-transfer salts, concentrating on the features that influence the magnetoresistance in high fields; a brief mention is also made of the deficiencies of bandstructure calculations. Magnetoresistive phenomena are discussed in Section 1.3, including measurements of the effective dimensionality, angle-dependent magnetoresistance oscillations (AMROs), the magnetoresistivity tensor and Fermi-surface-traversal resonances. The Shubnikov-de Haas effect is treated in Section 1.4, with a focus on the effects of reduced dimensionality and the extraction of quantities such as the quasiparticle scattering rate and effective mass. Sections 1.5 and 1.6 discuss some of the phenomena associated with charge-density waves above the Pauli paramagnetic limit. Finally, some thoughts about future prospects are given in Section 1.7.

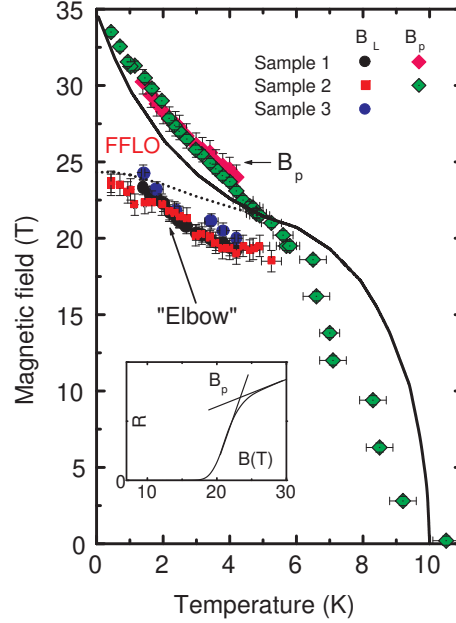


Fig. 1.1. Observation of the Fulde-Ferrel-Larkin-Ovchinnikov (FFLO) phase in $-(\text{BEDT-TTF})_2\text{Cu}(\text{NCS})_2$ [16]. The points labelled B_p denote the resistive upper critical field for two different samples (see inset for an illustrative example). The B_c points, denoting the phase boundary between the mixed phase and FFLO state were deduced using simultaneous MHz differential susceptibility measurements; the change in vortex stiffness that accompanies entry into the FFLO state causes an "elbow" in the field-dependent susceptibility. "Sample 3" is a measurement on a third sample under different conditions of electric field; consistency of the phase boundaries for the three samples shows that the effect is not due to artefacts of vortex pinning. The curves are a theoretical model due to Shimahara for the upper critical field and FFLO (see Ref. [16] for details).

1.2 Intralayer Fermi-surface topologies

The defining property of a metal is that it possesses a Fermi surface, that is, a constant-energy surface in k -space which separates the filled electron states from empty electron states at absolute zero ($T = 0$). The shape of the Fermi surface is determined by the dispersion relationships (energy versus k relationships) $E = E(k)$ of each partially-filled band and the number of quasiparticles to be accommodated. As is mentioned elsewhere in this book, the crystal structures of the organic metals and superconductors that feature in this article are mostly layered (or chain-like), with planes of anions (and perhaps other space-filling molecules [11,19]) alternating with layers of the cation molecules whose overlapping molecular orbitals provide the electronic bands. The main consequence of this structural anisotropy is that the

intralayer (or interchain) transfer integrals tend to be much greater by a factor 10^2 – 10^3 than the interlayer ones, so that most of the quasiparticle dispersion occurs parallel to the cation planes (or chains). Consequently, for many experiments, including the Shubnikov-de Haas and de Haas-van Alphen effects, the properties of the Fermi surface appear almost exactly two dimensional. We shall return to the consequences of this fact in later sections.

Figure 1.2 shows sections (parallel to the highly-conducting planes) through the first Brillouin zone and Fermi surfaces of two typical BEDT-TTF salts. The example in Figure 1.2 (a) is $-(\text{BEDT-TTF})_2\text{Cu}(\text{NCS})_2$ [20,22]; α -phase BEDT-TTF salts have a dimerized arrangement of BEDT-TTF molecules such that there are four per unit cell, each pair (or dimer) jointly donating one hole. The overall Fermi-surface cross-section is therefore the same as that of the Brillouin zone. However, the Fermi surface intersects the Brillouin zone boundaries in the c direction, so that band gaps open up (see e.g. Chapter 2 of Reference [24]). The Fermi surface thus splits into open (electron-like) sections (often known as Fermi sheets) running down two of the Brillouin-zone edges and a closed hole pocket (referred to as the “pocket”) straddling the other; it is customary to label such sections “quasi-one-dimensional” and “quasi-two-dimensional” respectively. The names arise because the group velocity v of the electrons is given by [23,24]

$$\vec{v} = \frac{1}{\hbar} \nabla_{\mathbf{k}} E(\mathbf{k}); \quad (1.1)$$

The Fermi surface is a surface of constant energy; Equation 1.1 shows that the velocities of electrons at the Fermi surface will be directed perpendicular to it. Therefore, referring to Figure 1.2, electrons on the closed Fermi-surface pocket can possess velocities which point in any direction in the (k_b, k_c) plane; they have freedom of movement in two dimensions and are said to be quasi-two-dimensional. By contrast, electrons on the open sections have velocities predominantly directed parallel to k_b and are quasi-one-dimensional.

α -phase BEDT-TTF superconductors $-(\text{BEDT-TTF})_2X$ can be made with a variety of other anion molecules, including $X = \text{Cu}[\text{N}(\text{CN})_2]\text{Br}$ (11.8 K), $\text{Cu}[\text{N}(\text{CN})_2]\text{Cl}$ (12.8 K (under pressure)), and I_3 (4 K); here the number in parentheses represents T_c . In all of these salts, the Fermi-surface topology is very similar to that in Figure 1.2 (a); small differences in the symmetry of the anion layer lead to variations in the gap between the quasi-one-dimensional and quasi-two-dimensional Fermi-surface sections [14,25,26]. A summary of the detailed differences and effective is given in Section 3.2 of Reference [14] (see also [25]). We shall see below (Section 1.3.3) that magnetic breakdown [14], in which the field-induced motion of quasiparticles causes them to tunnel across the gaps between the Fermi-surface sections, leading to new magnetic quantum oscillation frequencies, is a common phenomenon in these salts [67].

Figure 1.2 (b) shows the Fermi-surface topology and Brillouin zone of $-(\text{BEDT-TTF})_2\text{IBr}_2$ [27]. In this case (see Figure 1.2b) there is one hole per

unit cell, so that the Fermi surface cross-sectional area is half that of the Brillouin zone; only a quasi-two-dimensional pocket is present.

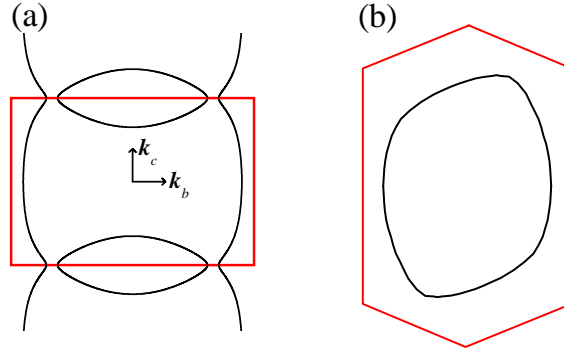


Fig. 1.2. (a) Brillouin zone and Fermi surface of $-(\text{BEDT-TTF})_2\text{Cu}(\text{NCS})_2$, showing the open, quasi-one-dimensional sections, and the closed, quasi-two-dimensional pocket [20,22]. (b) Brillouin zone and Fermi surface of $-(\text{BEDT-TTF})_2\text{IBr}_2$ [27].

As mentioned above, the bandstructure of a charge-transfer salt is chiefly determined by the packing arrangement of the cation molecules. The α , β , γ , and δ phases have tended to be the most commonly studied. The latter four phases all have predictable Fermi surfaces consisting of a quasi-two-dimensional pocket plus a pair of quasi-one-dimensional Fermi sheets (the pocket arrangement differs from phase to phase) [14,25,28]; the α -phase is alone in possessing a Fermi surface consisting of a single quasi-two-dimensional pocket [26].

As much of the rest of this article will be about using magnetoresistance to measure Fermi surfaces, it is worth including a brief note on the deficiencies of bandstructure calculations habitually applied to the organics. The bandstructures of crystalline organic metals have usually been calculated using the extended Hückel (tight-binding)¹ approach, which employs the highest occupied molecular orbitals (HOMOs) of the cation molecule [25]. Section 5.1.3 of Reference [26] discusses this approach and cites some of the most relevant papers. Whilst this method is usually quite successful in predicting the main features of the Fermi surface (e.g. the fact that there are quasi-one-dimensional and quasi-two-dimensional Fermi surface sections), the details of the Fermi surface topology are sometimes inadequately described (see e.g. [29]). This can be important when, for example, the detailed corrugations of a Fermi sheet govern the interactions which determine its low-temperature groundstate [20,29]. A possible way around this difficulty is to make slight

¹Simple introductions to the tight-binding model of bandstructure are given in References [23,24].

adjustments of the transfer integrals so that the predicted Fermi surface is in good agreement with experimental measurements [20{22,29]. In the α and β phases the predicted bandstructure seems very sensitive to the choice of basis set, and the disagreement between calculation and measurement is often most severe (see e.g. [30{33]).

More sophisticated Hubbard-unrestricted Hartree-Fock band calculations have been carried out for $-(\text{BEDT-TTF})_2\text{Cu}(\text{NCS})_2$ [34]. These calculations attempt to take into account many-body effects, and are successful in reproducing a number of experimental properties. They also indicate the importance of both antiferromagnetic fluctuations and electron-phonon interactions in $-(\text{BEDT-TTF})_2\text{Cu}(\text{NCS})_2$, a fact important in the proposed mechanisms for superconductivity [4,14]. More recently, techniques such as Dynamical Mean Field Theory (DMFT) have been applied to quasi-two-dimensional organic superconductors [4,35,36], predicting some aspects of the complex phase diagram of the β -phase BEDT-TTF salts.

1.3 High-field magnetotransport effects

1.3.1 Measurements of the effective Fermi-surface dimensionality via the SQUIT peak

We remarked above that the electronic properties of quasi-two-dimensional organic metals are very anisotropic. Many band-structure-measuring techniques chiefly give information about the intralayer topology of the Fermi surface. However, it is important to ask whether the Fermi surface is exactly two-dimensional, or whether it extends in the interlayer direction, i.e. is three-dimensional.

This question is of quite general interest, as there are many correlated-electron systems which have very anisotropic electronic bandstructure. In addition to the organic superconductors [14,37], examples include the "high- T_c " cuprates [38], and layered ruthenates [39] and manganites [40]. Such systems may be described by a tight-binding Hamiltonian in which the ratio of the interlayer transfer integral t_z to the average intralayer transfer integral t_{ij} is $\ll 1$ [14,37,41]. The inequality $\hbar\omega > \hbar t_z$ [42] where ω^{-1} is the quasiparticle scattering rate [37,38,41], frequently applies to such systems, suggesting that the quasiparticles scatter more frequently than they tunnel between layers. Similarly, under standard laboratory conditions, the inequality $k_B T > \hbar t_z$ often holds, hinting that thermal smearing will "wipe out" details of the interlayer periodicity [44].

The question has thus arisen as to whether the interlayer charge transfer is coherent or incoherent in these materials, i.e. whether or not the Fermi surface is a three-dimensional entity extending in the interlayer direction [14,37,41]. Incoherent interlayer transport is used as a justification

for a number of theories which are thought to be pivotal in the understanding of reduced-dimensionality materials (see e.g. [37,44]). Moreover, models for unconventional superconductivity in β -phase BEDT-TTF salts invoke the nesting properties of the Fermi surface [20,45,46]; the degree of nesting might depend on whether the Fermi surface is two dimensional or three dimensional (see [14], Section 3.5).

In this context, the experimental situation is at first sight complicated because many apparently solid experimental tests for coherence in organic metals and superconductors have been deemed to be inconclusive [41]; e.g. semiclassical models can reproduce AMRO [47] and FTR data [48,49] equally well when the interlayer transport is coherent or "weakly coherent" [41]. However, it turns out that magnetoresistance can yield an unambiguous measurement of interlayer coherence, by way of a feature in the interlayer magnetoresistivity ρ_{zz} known as the SQUIT (Suppression of Quasiparticle Interlayer Transport) or coherence peak, observed for exactly in-plane fields (Figs. 1.3 (a) and (b)).

To see how this comes about, consider a simple tight-binding expression for the interlayer (z-direction) dispersion [14,50]; $E(k_z) = -2t_z \cos(k_z a)$. Here t_z is the interlayer transfer integral and a is the unit-cell height in the z direction. The introduction of such an interlayer dispersion, paired with an in-plane two-dimensional dispersion relationship, will result in a three-dimensional Fermi surface with a sinusoidally-modulated Fermi-surface cross-section (see Ref. [24], Chapter 8). A more realistic version of the same idea is shown schematically for β -(BEDT-TTF)₂Cu(NCS)₂ in Figure 1.3 (c) [52,54,55] (compare Fig. 1.2 (a)). If the Fermi surface is extended in the interlayer direction, a magnetic field applied exactly in the intralayer plane can cause a variety of orbits on the sides of the Fermi surface (shown schematically in Fig. 1.3 (d) and (e)) via the Lorentz force

$$\hbar (d\mathbf{k}/dt) = -e\mathbf{v} \times \mathbf{B} \quad (1.2)$$

where \mathbf{v} is given by Equation 1.1; this results in orbits on the Fermi surface, in a plane perpendicular to \mathbf{B} [14,23]. Numerical modelling using a Chambers equation approach and a realistic parameterization of the Fermi surface [50] show that the closed orbits about the belly of the Fermi surface are very effective in averaging v_z , the interlayer component of the velocity. Therefore, the presence of such orbits will lead to an increase in the resistivity component ρ_{zz} [50,56,57]. On tilting \mathbf{B} away from the intralayer direction, the closed orbits cease to be possible when \mathbf{B} has turned through an angle θ , where [50]

$$(\text{in radians}) \quad \theta = v_z/v_{\parallel} \quad (1.3)$$

Here v_z is the maximum of the interlayer component of the quasiparticle velocity, and v_{\parallel} is the intralayer component of the quasiparticle velocity in the plane of rotation of \mathbf{B} . Therefore, on tilting \mathbf{B} through the in-plane orientation, one expects to see a peak in ρ_{zz} , of angular width 2θ , if (and only

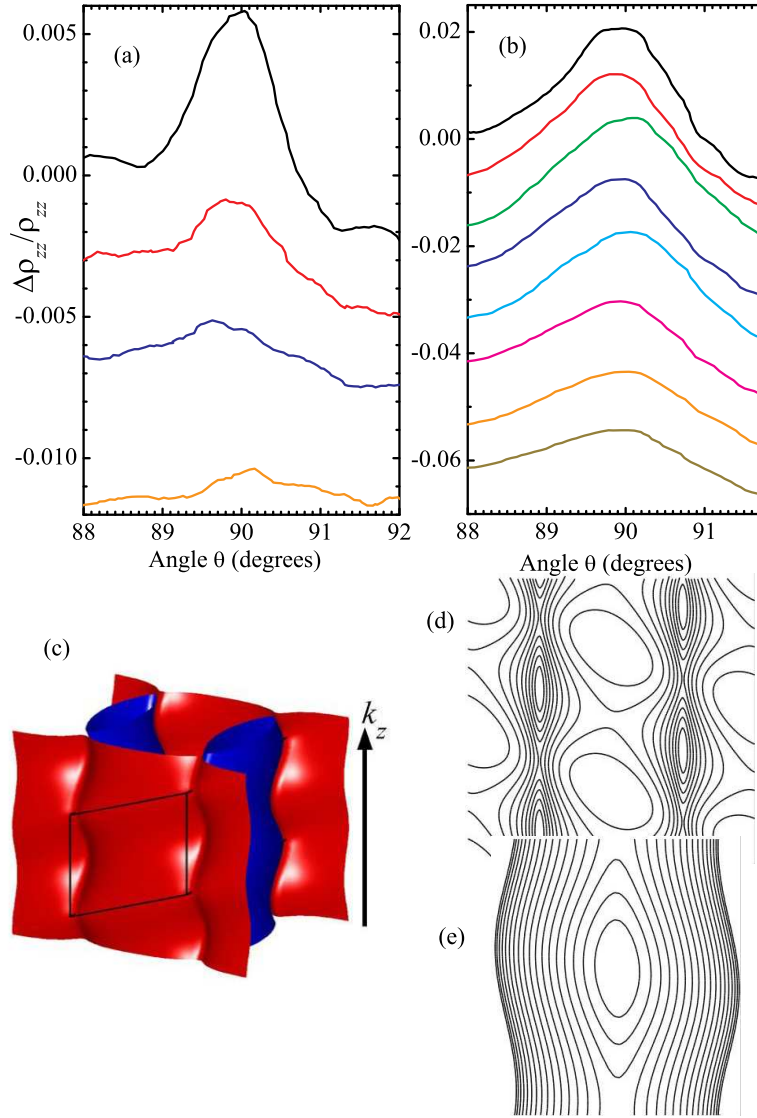


Fig. 1.3. Illustration of the "SQUIT" or "coherence peak" for in-plane fields in $-(\text{BEDT-TTF})_2\text{Cu}(\text{NCS})_2$ (after Ref. [51]). (a) The 45 T magnetoresistance of $-(\text{BEDT-TTF})_2\text{Cu}(\text{NCS})_2$ close to a tilt angle $\theta = 90^\circ$ plotted as $\Delta\rho_{zz}/\rho_{zz} = \rho_{zz}/\rho_{zzB} - 1$, the fractional change in ρ_{zz} from the more slowly-varying background. Data for temperatures $T = 5.3$ (highest), 7.6, 9.6 and 13.1 K (lowest) are shown, offset for visibility. In this plane of rotation, closed orbits on the quasi-one-dimensional Fermi-surface sections (see (d) below) are responsible for the SQUIT, observed as a peak at $\theta = 90^\circ$. (b) Similar data for a plane of rotation in which the SQUIT is caused by closed orbits on the quasi-two-dimensional Fermi-surface sections (see (e) below); the traces are for $T = 5.3$ (highest), 7.6, 8.6, 9.6, 10.6, 12.1, 13.1 and 14.6 K (lowest). Each trace has been offset for clarity. (c) Three-dimensional representation of the Fermi surface of $-(\text{BEDT-TTF})_2\text{Cu}(\text{NCS})_2$ (after Ref. [50]); the finite interlayer transfer integral gives the corrugations (shown greatly exaggerated) on the sides of the FS. Quasi-one-dimensional and quasi-two-dimensional Fermi-surface sections are shown in red and blue respectively. (d) Consequent field-induced closed orbits on the side of the quasi-one-dimensional Fermi-surface sections section when $\theta = 90^\circ$ and the field B is parallel to k_b . (e) Similar closed orbits on the quasi-two-dimensional section when $\theta = 90^\circ$ and B is parallel to k_c (see Fig. 1.2(a)). Orbits such as those in (d) and (e) give rise to the SQUIT peak in ρ_{zz} (see (a) and (b)).

if [41]) the Fermi surface is extended in the z direction. It is this peak that is referred to as the "coherence peak" or the "SQUIT" peak (Figs. 1.3 (a) and (b)). By using Equations 1.1 and 1.3 and measured details of the intralayer Fermi-surface topology, it is possible to use t_z to deduce t_z [50] to considerable accuracy.

Figures 1.3 (a) and (b) show typical data for $-(\text{BEDT-TTF})_2\text{Cu}(\text{NCS})_2$. The observation of a peak in ρ_{zz} close to $\theta = 90^\circ$ allows the interlayer transfer integral to be estimated to be $t_z \approx 0.065$ meV [50]. This may be compared with intralayer transfer integrals ≈ 150 meV [21].

Such data are of great interest because they illustrate that the criteria frequently used to delineate interlayer incoherence are rather a poor guide to reality. For example, a temperature of $T = 15$ K, ($k_B T \approx 30t_z$) leads one to expect incoherent interlayer transport via the criterion $k_B T > t_z$ proposed by Anderson [44], yet the peak in ρ_{zz} shown in Figure 1.3 (b) unambiguously demonstrates a three-dimensional Fermi-surface topology [51].

Demonstrations of interlayer coherence have been carried out on the quasi-two-dimensional organic conductors $-(\text{BEDT-TTF})_2\text{IBr}_2$ [27], $-(\text{BEDT-TTF})_2\text{Cu}_2(\text{CN})_3$ [58] (under pressure), $-(\text{BEDT-TTF})_2\text{NH}_4\text{Hg}(\text{SCN})_4$ [56] (under pressure), $-(\text{BEDT-TTF})_2\text{I}_3$ [56], $-(\text{BEDT-TTF})_2\text{Cu}(\text{NCS})_2$ [22], $-(\text{BETS})_2\text{GaCl}_4$ [33] and $-(\text{BEDT-TTF})_2\text{SF}_5\text{CH}_2\text{CF}_2\text{SO}_3$ [59,60]. In the latter example, no peak was observed, suggesting incoherent interlayer transport, or no warping. In all of the other instances, the ρ_{zz} data demonstrate a Fermi surface which is extended in the interlayer direction.

Inspired by this success, the technique has recently been extended to systems such as cuprate superconductors [62].

1.3.2 Mechanisms for angle-dependent magnetoresistance oscillations in quasi-two-dimensional organic metals

Whilst they give very accurate information about the cross-sectional areas of the Fermi-surface sections, magnetic quantum oscillations do not provide any details of their shape (see Section 1.4). Such information is usually derived from angle-dependent magnetoresistance oscillations (AMROs) [14,28,47,50,61]. AMROs are measured by rotating a sample in a fixed magnetic field whilst monitoring its resistance; the coordinate used to denote the position of AMROs is the polar angle between the normal to the sample's quasi-two-dimensional planes and the magnetic field [47,61]. It is also very informative to vary the plane of rotation of the sample in the field; this is described by the azimuthal angle [47,50,51,61].

As has been mentioned in the previous section, many quasi-two-dimensional charge-transfer salts of molecules such as BEDT-TTF and BETS exhibit the SQUIT or coherence peak, showing that they possess a well-defined three-dimensional Fermi surface, even at quite elevated temperatures [50]. In such cases, the AMROs can be modeled using a Boltzmann-transport approach

which treats the time-evolution of quasiparticle velocities across a three-dimensional Fermi surface².

In such a picture, AMROs result from the averaging effect that the semi-classical orbits on the Fermi surface have on the quasiparticle velocity. Both quasi-one-dimensional and quasi-two-dimensional Fermi-surface sections can give rise to AMROs; in the former case, the AMROs are sharp dips in the resistivity, periodic in \tan^{-1} ; in the latter case, one expects peaks, also periodic in \tan^{-1} [47, 61]. In order to distinguish between these two cases, it is necessary to carry out the experiment at several different θ (some *see* cautionary hints are given in Ref. [50]). The θ -dependence of the AMROs can be related directly to the shape of a quasi-two-dimensional Fermi-surface section; in the case of a quasi-one-dimensional sheet, the AMROs yield precise information about the sheet's orientation [14, 28, 47, 50, 61]. Typical data are shown in Figure 1.4. Numerical modelling of such data (using a Boltzmann transport approach) allows a detailed three-dimensional picture of the Fermi surface to be built up (*see* Figure 1.5(a)).

A third type of AMRO has been observed in the angle-dependent magnetoresistance of $-(\text{BEDT-TTF})_2\text{Cu}(\text{NCS})_2$ subjected to high pressures. The experiments employ a miniature diamond-anvil cell, attached to a cryogenic goniometer, providing full two axis rotation at ^3He temperatures [63]. The apparatus is placed in a 33 T Bitter magnet. A plethora of AMROs is observed at each pressure (Figure 1.5(b)), caused by field-induced quasiparticle orbits across the Fermi surface. Raising pressure suppresses the gap between the quasi-two-dimensional pocket and quasi-one-dimensional sheets of the Fermi surface (*see* Figure 1.2(a)), increasing the probability of magnetic breakdown (*see* Section 1.3.3 and Ref. [67] for a more detailed explanation of magnetic breakdown). This permits AMROs due to breakdown orbits about the complete Fermi surface.

Finally, note that increasing the temperature gradually suppresses the AMROs (*see* Figures 1.6(a) and (b)). Modelling of this phenomenon shows that it can be described by a temperature-dependent scattering rate, $\tau^{-1} = \tau_0^{-1} + T^2$, where τ_0 and τ_1 are constants [51]. The exponent suggests that the suppression of AMROs is due to electron-electron scattering. Another interesting feature of this suppression is that the same scattering rate appears to apply to orbits on the quasi-one-dimensional and quasi-two-dimensional parts of the Fermi surface. This suggests that mechanisms for superconductivity in organic metals that invoke a large variation in scattering rate over the FS (e.g. FLEX methods [20]) may be inappropriate for $-(\text{BEDT-TTF})_2\text{Cu}(\text{NCS})_2$.

²As mentioned elsewhere in this book, the picture for TM T SF salts can be rather different.

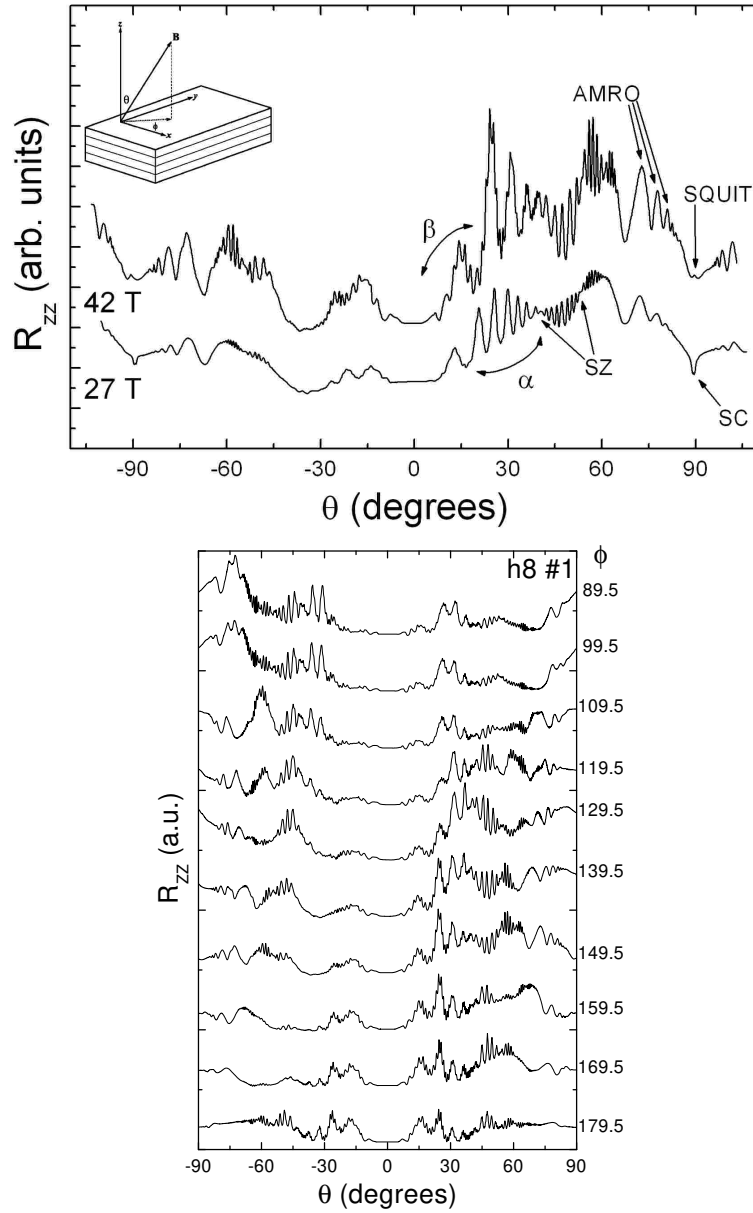


Fig. 1.4. (a) Typical dependence of the magnetoresistance of $(\text{BEDT-TTF})_2\text{Cu}(\text{NCS})_2$ [50]. The data shown are for a hydrogenated sample at 490 mK, $\phi = 149^\circ$ (where ϕ is the azimuthal angle) and fields of 27 T (lower), and 42 T (upper). The data have been offset for clarity. Some representative features are indicated; Shubnikov-de Haas (SdH) oscillations due to the Q2D pockets (β) and the breakdown orbit (α); spin zeros in the SdH amplitudes (SZ); the onset of the superconducting transition (SC); angle-dependent magnetoresistance oscillations (AMRO), whose positions are field independent; and the resistive SQUIT peak in the presence of an exactly in-plane magnetic field (in-plane Peak). The inset diagram is included to illustrate the measurement geometry. (b) The angle-dependent interlayer magnetoresistance of the same sample at various values of the azimuthal angle ϕ ; $T = 500$ mK and $B = 42$ T.

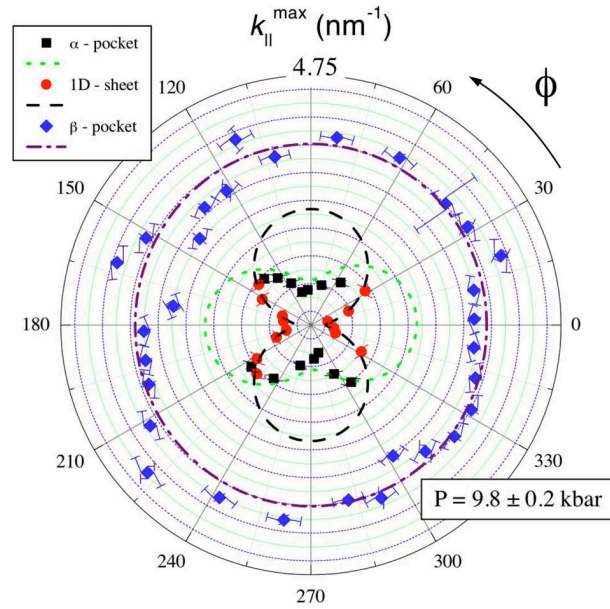
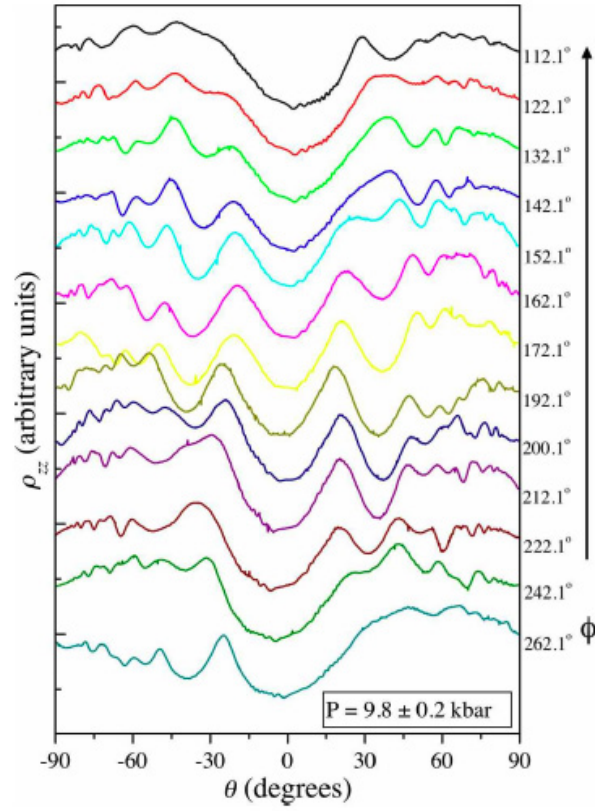


Fig. 1.5. Top: typical angle-dependent magnetoresistance oscillations (AMROs) at a magnetic field of 30 T and a temperature of 1.5 K; the pressure is 9.8 kbar. Here, θ denotes the angle between the normal to the sample's quasi-two-dimensional planes and the field; ϕ describes the plane of rotation. Bottom: polar plot of the periodicities (in units of nm^{-1}) of the various AMRO series. The inset key gives the mechanism for the features, with the blue diamonds representing the oscillations due to magnetic breakdown [63].

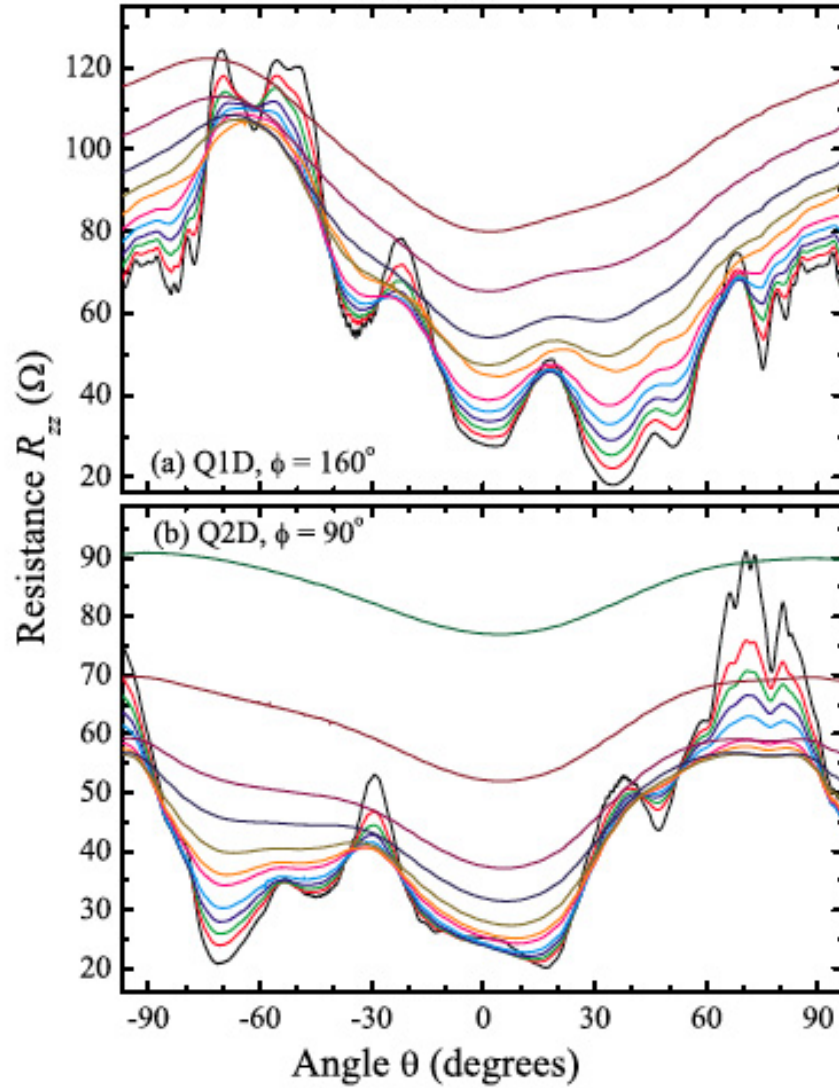


Fig. 1.6. Suppression of AMROs by increasing temperature shown as interlayer resistance R_{zz} (Ω) of a $-(BEDT-TTF)_2Cu(NCS)_2$ crystal versus tilt angle for various constant T ($B = 45$ T). (a) Data for $\phi = 160^\circ$, a plane of rotation at which R_{zz} is determined by phenomena on the quasi-one-dimensional Fermi-surface sections. In order of increasing R_{zz} at $\theta = 35^\circ$, the curves are for $T = 5.3, 6.5, 7.6, 8.6, 9.6, 10.6, 12.1, 13.1, 14.6, 17.1, 19.6$ and 29.3 K respectively. (b) Similar data for $\phi = 90^\circ$; here R_{zz} features are associated with the quasi-two-dimensional Fermi-surface. In order of increasing R_{zz} at $\theta = 70^\circ$, the curves are for $T = 5.3, 7.6, 8.6, 9.6, 10.6, 12.1, 13.1, 14.6, 17.1, 19.6, 24.5$ and 29.3 K respectively.

1.3.3 Further clues about dimensionality in the resistivity tensor components

In the past there has been some confusion as to the origin of AMROs in quasi-two-dimensional charge-transfer salts of BEDT-TTF; and in particular, the component of the resistivity tensor in which the oscillations occur. There are few reliable measurements of the in-plane conductivity or resistivity ρ_{xx} of quasi-two-dimensional crystalline organic metals [3,14]; experiments involving conventional edge contacts are problematic [3,14]. Because of the very large resistivity anisotropy, such data are almost often dominated by the much larger interplane resistivity component, ρ_{zz} [14]. In order to circumvent this problem, a number of authors have turned to a MHz skin depth technique to measure the field dependence of the in-plane resistivity [3,33,64,65]; this technique is very suitable for pulsed magnetic fields [3,33,65]. Samples for such experiments are mounted within a small coil which forms part of the tank circuit of a tunnel-diode oscillator; shifts in frequency can be related to changes in the skin depth and hence to changes in the in-plane conductivity [33,64]. In some experiments [3,64], top and bottom contacts are also mounted on the sample, so that simultaneous measurements of the interplane resistivity component, ρ_{zz} can be made.

Figure 1.7 shows a comparison of ρ_{zz} and the frequency shift, measured simultaneously. The most noticeable contrast between the two data sets is the much more prominent magnetic breakdown (the higher frequency) oscillations in the (in-plane) frequency data. Although a quantitative model of such oscillations poses some theoretical difficulties, it is easy to see qualitatively why magnetic breakdown will influence the in-plane conductivity much more than it does the interplane conductivity. Magnetic breakdown represents the tunnelling of quasiparticles from the one Fermi-surface section to another [67]. This will affect the way in which a quasiparticle's velocity evolves with time, and hence the conductivity. As virtually all of the dispersion of the electronic bands is in-plane, a magnetic breakdown event will have a relatively large effect on the time dependence of the in-plane component of a quasiparticle's velocity. By contrast, the warplings in the interplane direction of both sections of the Fermi surface of $-(\text{BEDT-TTF})_2\text{Cu}(\text{NCS})_2$ seem to be rather similar [22]; hence magnetic breakdown will have comparatively little effect on the time evolution of the interplane component of the quasiparticle velocity.

Figure 1.8 contrasts the angle dependence of the two components of the resistivity at fixed magnetic field. Whereas ρ_{zz} exhibits strong AMROs, the frequency (depending on the in-plane resistivity) shows none. This is entirely consistent with the expectations of semiclassical models of AMROs [47,50].

It should be noted that a high-frequency variant of AMROs, known as the Fermi-surface-traversal resonance (FTR), has been developed. This high-frequency (GHz) magneto-optical technique allows additional information

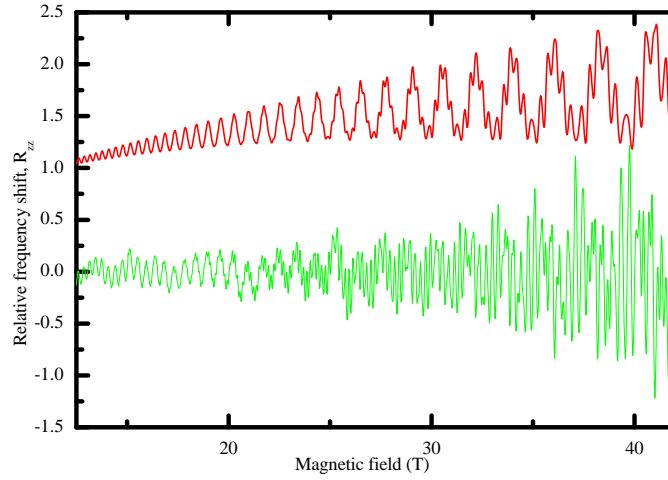


Fig. 1.7. Simultaneous measurement of R_{zz} (upper trace) and the frequency shift of a tunnel diode oscillator (related to the in-plane component of the resistivity) (lower trace). The sample is a single crystal of $-(\text{BEDT-TTF})_2\text{Cu}(\text{NCS})_2$; the temperature is 470 mK. Note that the rapid magnetic quantum oscillations due to magnetic breakdown are much more prominent in the lower data set. (After Ref. [49].)

about the topology and corrugations of quasi-one-dimensional Fermi sheets to be deduced [14,48,68].

1.4 High-field Shubnikov-de Haas measurements and quasiparticle scattering.

Above we saw that the effect of the small but finite interlayer transfer integral on the Fermi-surface topology is very important in phenomena such as angle-dependent magnetoresistance oscillations (AMROs). However, from the perspective of magnetic quantum oscillatory phenomena such as the Shubnikov-de Haas and de Haas-van Alphen effects, the Fermi surface properties behave in an almost ideally two-dimensional way. To see how this occurs, consider the Landau quantization of the quasiparticle states due to a magnetic field B : [23,24]

$$E(B; k_z; l) = \frac{\hbar e B}{m} \left(l + \frac{1}{2} \right) + E(k_z) \quad \sim \hbar \omega_c \left(l + \frac{1}{2} \right) + E(k_z): \quad (1.4)$$

Here $E(k_z)$ is the energy of the (unmodified) motion parallel to B , l is the Landau quantum number ($0; 1; 2; \dots$) and m is an orbitally-averaged effective mass; the angular frequency $\omega_c = eB/\hbar m$ (the cyclotron frequency) corresponds to the semiclassical frequency at which the quasiparticles orbit

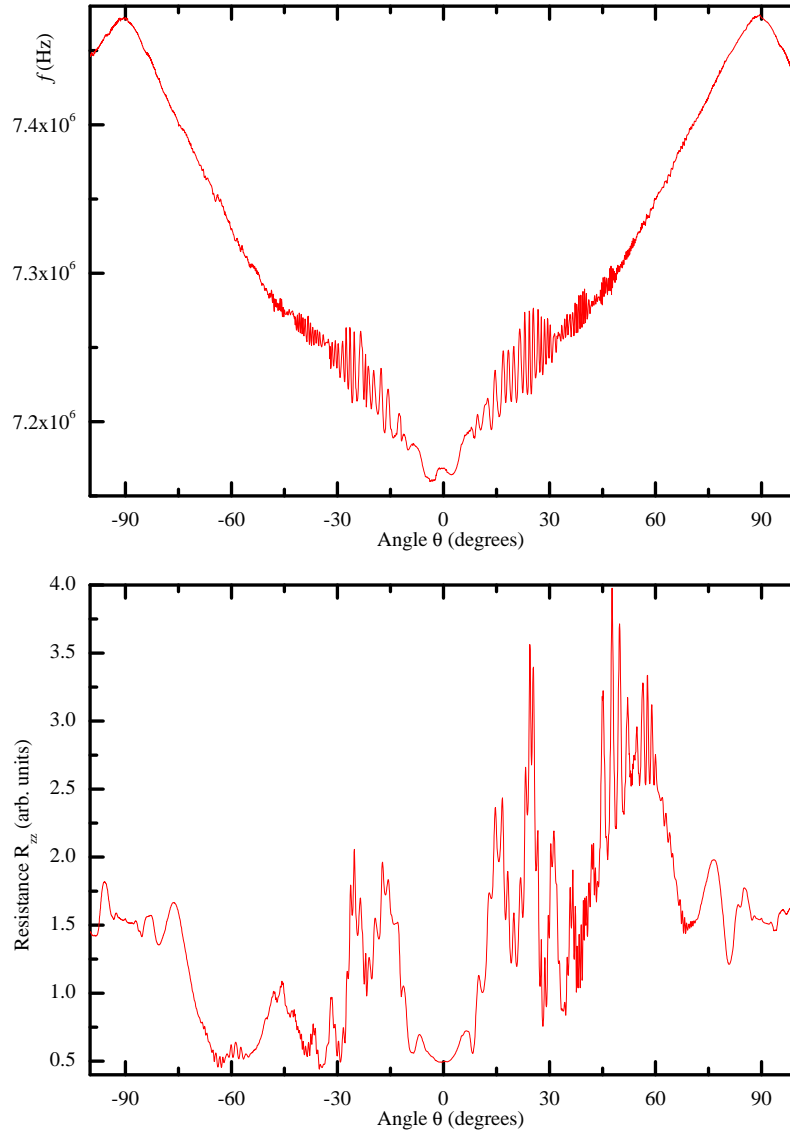


Fig. 1.8. Comparison of the magnetic-field orientation dependence of the interlayer resistance R_{zz} (lower trace—proportional to χ_{zz}) and that of the frequency shift of a tunnel diode oscillator (upper trace—related to ω_{jj}) measured simultaneously. $\theta = 0$ corresponds to the field being normal to the quasi-two-dimensional planes of $-(\text{BEDT-TTF})_2\text{Cu}(\text{NCS})_2$. The temperature is 470 mK and the static magnetic field is 42 T. The rapid oscillations close to $\theta = 0$ in both figures are Shubnikov-de Haas oscillations. The slower oscillations, periodic in $\tan \theta$, and only seen in the lower trace, are AMROs. The peak denoting interlayer coherence is visible at $\theta = 90$ in the lower figure (after Reference [49]).

the Fermi surface [23,24]. (For the moment we neglect the Zeeman term due to spin [14].) In virtually all practical experiments, the magnetic field is perpendicular to the highly-conducting planes or tilted by angles less than 60° from this direction. In such situations, $E(k_z)$ will be $\approx \hbar v_F$; for most of the quasi-two-dimensional charge-transfer salts, the Landau-level energy spacing will eclipse $\hbar v_F$ in fields of order 1–5 T. The necessity to use a rigorously two-dimensional approach to analyse the Shubnikov-de Haas (resistivity) and de Haas-van Alphen (magnetization) oscillations [14,28,69] in these cases cannot be overemphasized; see References [66,67] for a thorough discussion of this point.

1.4.1 The deduction of quasiparticle scattering rates

Recently, it has been proposed that the dependence of superconducting properties on the quasiparticle scattering rate is an excellent way of identifying the mechanism for superconductivity in quasi-two-dimensional organics [1]. Unfortunately, this is not as straightforward as it might seem. A measure of the scattering rate in metallic systems is often derived from the rate at which magnetic quantum oscillations (such as de Haas-van Alphen oscillations) grow in amplitude with increasing magnetic field; the dominant term in the Lifshitz-Kosevich formula (see e.g. Refs. [66,69]) describing this phenomenon is $\exp[-14.7 m_{CR} T_D / B]$ (SI units). The constant describing the phase-smearing of the oscillations due to Landau-level broadening is the so-called Dingle temperature, T_D .

If one were to assume that T_D is due solely to scattering (i.e. the energy width of the Landau levels detected by the de Haas-van Alphen effect is associated only with their finite lifetime due to scattering) then T_D would be related to the scattering rate $\frac{1}{\tau_{dHvA}}$ by the expression

$$T_D = \frac{\hbar}{2 k_B \tau_{dHvA}} : \quad (1.5)$$

In many experimental works, it is assumed that the τ_{dHvA} deduced from T_D in this way is a true measure of scattering rate; however, in quasi-two-dimensional organic metals this is almost certainly not the case. The problem becomes apparent if such scattering times are compared with the τ_{CR} deduced from cyclotron resonance experiments [49]. In such cases the following inequality is found;

$$\tau_{CR} > \tau_{dHvA} : \quad (1.6)$$

For some layered metals (see, for example, the work of Hill [70]), the τ_{CR} measured in cyclotron resonance has been found to be four to ten times larger than τ_{dHvA} ; An example of this is shown in Figure 11 of Ref. [49], where the insertion of the scattering rate inferred from Shubnikov-de Haas oscillations into a model for the cyclotron resonance produces linewidths that are much too broad. A more realistic linewidth is obtained with a longer scattering

time. As we shall now describe, spatial inhomogeneities are the likely culprit for the difference of scattering times.

Screening is less effective in systems containing low densities of quasiparticles (such as organic metals), compared to that in elemental metals; hence variations in the potential experienced by the quasiparticles can lead to a spatial variation of the Landau-level energies (see Figure 1.9). Even in the (hypothetical) complete absence of scattering, Harrison [71] has shown that this spatial variation would give the Landau level a finite energy width (see Figure 1.9) and therefore lead to an apparent Dingle temperature

$$T_D = \frac{x [1 - x] F^0(x)^2 a}{k_B m} \frac{\hbar}{2F} : \quad (1.7)$$

Here F is the magnetic-quantum-oscillation frequency, and $F^0 = dF/dx$; x represents the (local) fractional variation of the quasiparticle density due to the potential fluctuations and \bar{x} is its mean.

The Dingle temperature measured in experiments will therefore usually represent a combination of the effects described by Equations 1.5 and 1.7. Hence the simple-minded use of Equation 1.5 to yield τ_{dHvA} from T_D will tend to result in a parameter that is an overestimate of the true scattering rate (see Figure 1.9). By contrast, cyclotron resonance (shown by vertical arrows in Figure 1.9) is a "vertical" transition (due to the very low momentum of the photon); it will measure just the true width of the Landau levels due to scattering (represented by shading) [49].

Providing a thorough treatment of the sample's high-frequency magnetoconductivity is made [49], then the measured scattering rate deduced from a cyclotron resonance experiment is a good measure of the energy width of the Landau levels due to their finite lifetime. Once this has been realized, cyclotron resonance can be used to give quantitative details of the quasiparticle scattering mechanisms. By contrast, the apparent scattering rate deduced from de Haas-van Alphen and Shubnikov-de Haas oscillations can contain very significant contributions from spatial inhomogeneities [71].

Finally, one should add that the scattering rate τ^{-1} measured in a zero-field in-plane conductivity experiment can be very significantly different from τ_{CR}^{-1} because the two measurements are sensitive to different types of scattering process. One of us has discussed this issue in detail in two recent papers [72,73]; in particular, in the case of the α -phase BEDT-TTF salts, there is an (as-yet) unexplained quantitative discrepancy between the size of the in-plane conductivity and other measures of the quasiparticle properties [73]. Further work to resolve this question is necessary.

Finally, "jitter" in the Brillouin zone boundary may be yet another source of scattering. This is predicted to give rise to 'hot spots' where the Fermi surface intersects the Brillouin zone boundary [74].

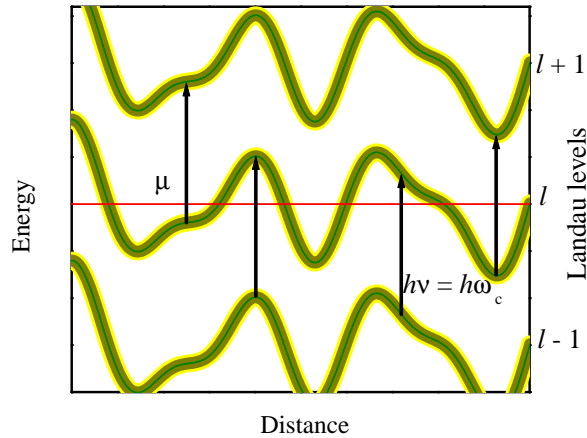


Fig. 1.9. Cartoon of the effect of spatial inhomogeneities on Landau-level widths and energies. The variations in the potential experienced by the electrons make the Landau levels (shaded curves) move up and down in energy as one moves through the sample. As the field is swept, the levels will move up through the chemical potential and depopulate, resulting in the de Haas-van Alphen and Shubnikov-de Haas effects. The Dingle Temperature essentially parameterizes the movement of the total energy width of a Landau level through μ ; hence it will measure a width that includes the energy variation due to inhomogeneities. By contrast, cyclotron resonance (shown by vertical arrows) is a "vertical" transition; it will measure just the true width of the Landau levels due to scattering (represented by shading).

1.5 Charge-density waves at fields above the Pauli paramagnetic limit

Intense magnetic fields (B) impose severe constraints on spin-singlet paired electron states. Superconductivity is one example of a groundstate where this is true, although orbital diamagnetic effects usually destroy superconductivity at lower magnetic fields than does the Zeeman effect [16,75]. Charge-density wave (CDW) systems, by comparison, are mostly free from orbital effects [76], and so can only be destroyed by coupling B directly to the electron spin. While most CDW systems have gaps that are too large to be destroyed in laboratory-accessible fields [76], several new compounds have been identified within the last decade that have gaps ($2\Delta_0$) as low as a few meV, bringing them within range of state-of-the-art static magnetic fields.

As we shall discuss in Section 1.6, $-(\text{BEDT-TTF})_2\text{Mg}(\text{SCN})_4$ (where $M = \text{K, Tl or Rb}$; $2\Delta_0 \approx 4$ meV) is one example that has been extensively studied [77]. However, it has a complicated phase diagram in a magnetic field owing to the imperfect nature of the nesting [78]; closed orbits exist after the Fermi-surface reconstruction which become subject to Landau quantization in a magnetic field [79], potentially modifying the groundstate. By contrast,

$(\text{Per})_2\text{M}(\text{mnt})_2$ (where $\text{M} = \text{Pt}$ and Au) appears to be fully gapped [80]. However, the existence of spin $\frac{1}{2}$ moments on the Pt sites makes the $\text{M} = \text{Au}$ system a pristine example of a small-gap, fully dielectric CDW material.

Measurements of the CDW transition temperature T_P (where the subscript "P" stands for "Peierls") in $(\text{Per})_2\text{Au}(\text{mnt})_2$ ($T_P = 11\text{ K}$ at $B = 0$) as a function of B indicate that it is suppressed in a predictable fashion [81], allowing a Pauliparamagnetic limit of $B_P = 37\text{ T}$ to be inferred. However, the closure of the CDW gap with field is in fact considerably more subtle [82]; a finite transfer integral t_a perpendicular to the nesting vector produces a situation analogous to that in an indirect-gap semiconductor, where the minimum energy of the empty states above the chemical potential is displaced in k -space from the maximum-energy occupied states below [82]. Consequently, Landau quantization of the states above and below is possible, leading to a thermodynamic energy gap $E_g(B; T)$ of the form [82]

$$E_g(B; T) = 2(T) + 4t_a g_B B + \frac{1}{2}\hbar\omega_c \quad (1.8)$$

Here, (T) is the temperature-dependent CDW order parameter ($(T) \rightarrow 0$ as $T \rightarrow 0$), ω_c is a characteristic cyclotron frequency in the limit $B \rightarrow 0$, and g is a nonparabolicity factor; $g_B = 2$ is the Lande g -factor and $\hbar\omega_c$ is the Bohr magneton. Note that the Landau quantization competes with Zeeman splitting; however, at sufficiently high B it becomes impossible to sustain closed orbits, leading to a straightforward dominance of the Zeeman term [82].

Another subtlety in assessing the field-dependent thermodynamic gap (and hence the Pauliparamagnetic limit) in $(\text{Per})_2\text{Au}(\text{mnt})_2$ stems from the complicated nature of the low-temperature electrical conductivity, which contains contributions from both the sliding collective mode of the CDW and thermal excitation across the gap (see Fig. 1.10(a)) [82, 83]. This leads to a measured resistivity $\rho_{yy} = (j_y / E_t)^{-1}$, where j_y is the conductivity due to thermal excitation across the gap and $j_y = E_t$ is the contribution from the collective mode, j_y being the current density and E_t the threshold electric field to depin the CDW. Now Eq. 1.8 contains E_g , which is T -dependent; moreover, E_t may also depend on T . Thus, Arrhenius plots are in general curved (see Fig. 1.10(b)), with a slope

$$\frac{\partial \ln \rho_{yy}}{\partial (1/T)} = \frac{\frac{1}{2k_B} (E_g + T \frac{\partial E_g}{\partial T}) + \frac{j_y T^2}{T E_t^2} \frac{\partial E_t}{\partial T}}{1 + \frac{j_y}{T E_t}} \quad (1.9)$$

With appropriate choice of temperature and bias regimes, it is possible to make a reliable estimate of E_g from plots such as those in Fig. 1.10(b). On the other hand, it can be shown [84] that poorly-chosen experimental conditions can easily lead to errors in the size of the derived gap.

Once accurate values of $E_g(B)$ have been obtained, the method of Ref. [82] can be used to fit Eq. 1.8 by adjusting the parameters $2(T) + 4t_a$, $4t_a$ and v_F , where v_F is the Fermi velocity in the metallic state; in the CDW state

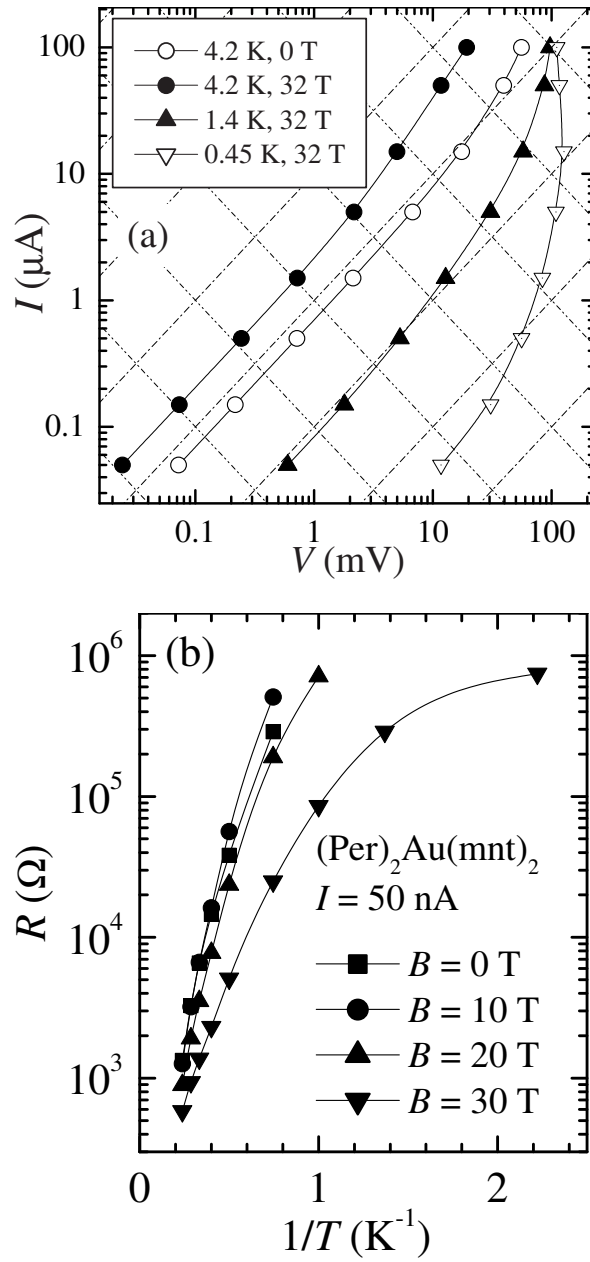


Fig. 1.10. (a) Non-linear current-versus-voltage characteristics of $(\text{Per})_2\text{Au}(\text{mnt})_2$ plotted on a logarithmic scale for various temperatures and fields (see inset key). The negative-slope diagonal lines are contours of constant power and the positive-slope diagonal lines are contours of constant resistance, providing a guide as to when the sample's behavior is dominated by ohmic, thermally-activated conduction rather than sliding. (b) Arrhenius plots of resistance R (in Ω , logarithmic scale) versus $1/T$ with $I = 50 \text{ nA}$ for $(\text{Per})_2\text{Au}(\text{mnt})_2$ at several different B (after Ref. [82]).

it is used to parameterise the quasiparticle dispersion. A good fit is obtained using $t_a = 0.20 \pm 0.01$ meV, $v_F = (1.70 \pm 0.05) \times 10^8$ m s⁻¹ and $2\epsilon_0 = 4.02 \pm 0.04$ meV [82]. These parameters correspond to $E_g = 3.21 \pm 0.07$ meV at $B = 0$, $T = 0$; the derived transfer integrals t_a and t_b (≈ 188 meV) are in good agreement with theory [85] and thermopower data [80]. (Note that these band parameters exclude the possibility of field-induced CDW (FICDW) states of the kind proposed in Ref. [86] in $(\text{Per})_2\text{Mn}(\text{mnt})_2$ salts.)

Armed with the band parameters, one obtains a reliable estimate of the Pauli paramagnetic limit; $B_P = (\epsilon_0 + 2t_a)/2gs_B \approx 30$ T. This corresponds to a sharp drop in measured resistance R_{xx} , as shown in Fig. 1.11 (left side), which displays data recorded at $T = 25$ mK. At such temperatures, there are very few thermally-activated quasiparticles indeed, leaving only the CDW collective mode to conduct; this gives rise to a R_{xx} in Fig. 1.11 that is strongly dependent on current. On passing through $B_P \approx 30$ T, R_{xx} drops very sharply, and there is also hysteresis between up- and down-sweeps of the field. The latter effect could be the consequence of a first-order phase transition on reaching B_P , compounded by CDW pinning effects.

However, the most interesting observation about Fig. 1.11 is the fact that the strongly non-linear $I-V$ characteristics persist at fields well above B_P , as can be seen from both R_{xx} data and $I-V$ plots (right-hand side of Fig. 1.11). One can conclude from these data that it is the CDW depinning voltage that changes at B_P . This is probably a consequence of the CDW becoming incommensurate or of the order parameter of the charge modulation becoming considerably weakened [76, 83]. Evidence for the latter is obtained by repeating the $I-V$ measurements at slightly higher temperatures of 900 mK (Fig. 1.11, right side). This temperature is sufficient to restore Ohmic behaviour for $B > B_P$, suggesting that a reduced gap for $B > B_P$ allows quasiparticles to be more easily excited.

There have been some interesting proposals for FICDW phases (e.g. Ref. [86]). These mechanisms require the system not to be completely gapped; instead possessing a closed orbit for one of the spins which would then have a Landau gap at the chemical potential. Such a situation typically leads to the quantum Hall effect, and a metallic behaviour of longitudinal resistivity [88]. Current would then be able to flow without the CDW having to be depinned. These effects nevertheless appear to be absent from the data of Fig. 1.11; the continuation of the non-linear CDW electrodynamics for $B > B_P$ suggests that metallic behaviour is not regained. Instead, both spin components of the Fermi surface are most likely to be gapped independently with differing nesting vectors, leading to an exotic CDW phase that has some analogies with the FFLO state of superconductors. The presence of two distinct, spin-polarized CDWs with different periodicities will furnish separate spin and charge modulations that could in principle be detected using a diffraction experiment [83].

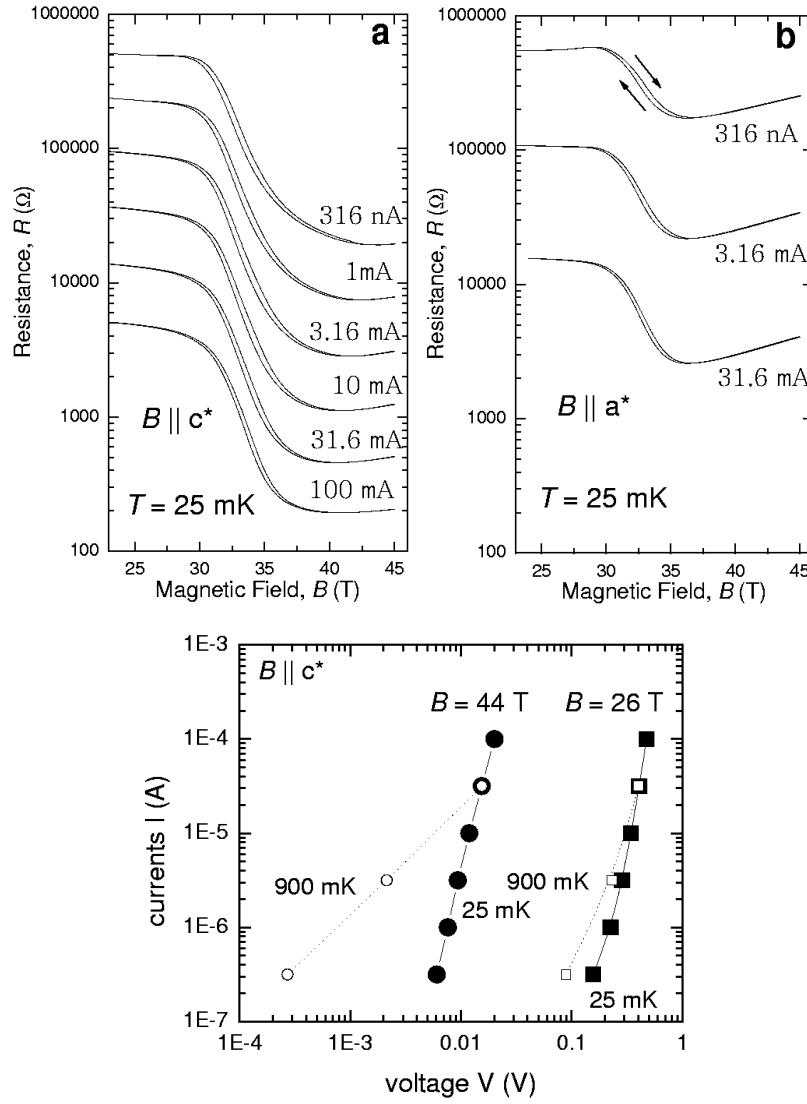


Fig. 1.11. Top: resistance of a single crystal of $(\text{Per})_2\text{Au}(\text{mnt})_2$ measured at 25 mK for fields between 23 and 45 T, for two different orientations c^* (a) and a^* (b) of B perpendicular to its long axis b , at several different applied currents. The lowest resistance for a given current occurs for B parallel to c^* , which is perpendicular to a^* . The dependence of the resistance on current signals non-ohmic behaviour. Bottom: non-linear current-versus-voltage characteristic of $(\text{Per})_2\text{Au}(\text{mnt})_2$ plotted on a log-log scale, for magnetic fields (26 and 44 T) above (circles) and below (squares) B_F . Filled symbols connected by solid lines represent data taken at 25 mK while open symbols connected by dotted lines represent data taken at 900 mK. (After Ref. [33].)

It has been suggested [87] that FICDWs occur in charge-density wave (CDW) systems in strong magnetic fields when orbital quantization facilitates nesting of quasi-one-dimensional Zeeman-split bands. The free energy is minimised at low integral Landau subband filling factors by the formation of a Landau gap at the Fermi energy [87]. Hence, as is the case in field-induced spin-density wave states (FISDW) [88], orbital quantization is implicit in FICDW formation, yielding a Hall conductivity $\sigma_{xy} = 2e^2/h$ (where $a = 20 \text{ \AA}$ is the layer spacing) and a longitudinal conductivity $\sigma_{xx} = \sigma_0 \exp[-k_B T]$ that is very small and thermally activated ($\sigma_{xx} = \sigma_{xy}$). Inversion of the conductivity tensor yields

$$\sigma_{xx} = (2e^2/h)^2 \sigma_0 e^{-k_B T} \quad \sigma_{xy} = 2e^2/h \quad (1.10)$$

$$\sigma_{xx} = (\sigma_0)^+ e^{-k_B T} \quad \sigma_{xy} = 0 \quad \sigma_{xx} = 0 \quad \sigma_{xy} = 0 \quad (1.11)$$

Samples of $(\text{Per})_2\text{Pt}(\text{mnt})_2$ have the ideal topology ($1000 \text{ m} \times 50 \text{ m} \times 25 \text{ m}$) for deriving reliable estimates of σ_{xx} from the R_{xx} data of Ref. [86], yielding $130 \times 10^{-6} \text{ cm}$, greatly exceeding the maximum metallic resistivity $\sigma_{xx} = 2e^2/h \approx 26 \text{ cm}$ throughout all of the proposed FICDW phases by as much as a factor of 20000. The data of Ref. [86] are therefore consistent with $\sigma_{xx} = 0$ throughout. For the quantized nesting model to apply, each FICDW state would have different values of σ_{xx} , only one of which can be 0.

Varying the current, I , causes R_{xx} and thus σ_{xx} vary considerably, reaching values in Fig. 1.1a that exceed $\sigma_{xx} = 2e^2/h$ by a factor $\sim 10^7$. Its strong dependence on the current density j is consistent with a sliding collective mode contribution to σ_{xx} (for all fields $B < 33 \text{ T}$ and $\sigma_{xx} = 0$), yielding

$$\sigma_{xx} = [\sigma_0 \exp(-k_B T) + j/E_t]^{-1}; \quad (1.12)$$

where E_t is a threshold CDW depinning electric field [90], that may itself depend on T . Note that the near-linear I versus voltage V plots for $IV < 2 \text{ W}$ (for different values of B , T and I in Fig. 2 of Ref. [90]) suggests that heating is not a significant factor for $I < 5 \text{ A}$ in Fig. 1.12a.

Hence, the behavior of the fully gapped $(\text{Per})_2\text{M}(\text{mnt})_2$ system does not fit the usual definition of "magnetoresistance" but is the consequence of magnetic field-induced changes in the electric field E_t required to depin the CDW from the lattice, where $\sigma_{xx} = 0$ throughout. Such behavior is inconsistent with the quantized nesting model which requires different values of σ_{xx} for each sub-phase [87]; thus the steps in σ_{xx} probably correspond to field-induced changes in E_t .

The cooperative dimerization of the Pt spins in $(\text{Per})_2\text{Pt}(\text{mnt})_2$ can easily provide a mechanism for additional phase transitions or changes in E_t compared to $(\text{Per})_2\text{Au}(\text{mnt})_2$. The Pt spins couple strongly to both the CDW, via distortions of the crystal lattice, and B , as shown by the fact that they dominate the total magnetic susceptibility (Fig. 1.12(b)). Their effect on the phase diagram is likely to be significant until all spins are fully aligned by a field $B \approx 40 \text{ T}$ (Fig. 1.1(b)).

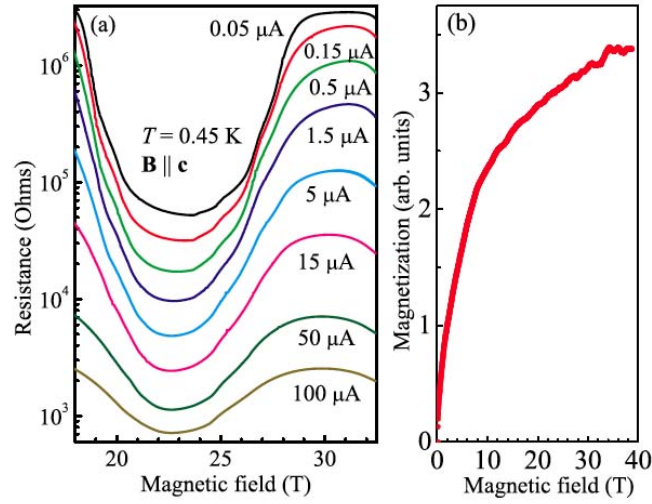


Fig. 1.12. (a) Resistance versus field for $(\text{Per})_2\text{Pt}(\text{mnt})_2$ at various currents measured by the present authors. (b) Magnetization M of many randomly oriented $(\text{Per})_2\text{Pt}(\text{mnt})_2$ crystals at $T = 0.50$ K; M does not saturate by $B = 40$ T [90].

1.6 A new quantum fluid in strong magnetic fields with orbital flux quantization

$-(\text{BEDT-TTF})_2\text{KHg}(\text{SCN})_4$ is undoubtedly one of the most intriguing of BEDT-TTF-based charge-transfer salts [77–79]. Like many other such materials, it possesses both two-dimensional (2D) and one-dimensional (1D) Fermi-surface (FS) sections. However, the 1D sheets are unstable at low temperatures, causing a structural phase transformation below $T_p = 8$ K into a CDW state [88]. Im perfect nesting combined with the continued existence of the 2D hole FS pocket gives rise to complicated magnetoresistance and unusual quantum-oscillation spectra at low magnetic fields and low temperatures [14]. At high fields, the CDW undergoes a number of transformations into new phases, many of which have been suggested to be field-induced CDW phases [78].

Undoubtedly the most exotic aspect of this material is its transformation into an unusual CDW state above a characteristic field $B_k = 23$ T (known as the “kink” transition); B_k is now known to correspond to the CDW Pauli paramagnetic limit [14, 79], like $(\text{Per})_2\text{M}(\text{mnt})_2$. Such a regime is reached in $-(\text{BEDT-TTF})_2\text{KHg}(\text{SCN})_4$ owing to the unusually low value of T_p [79]. At fields higher than B_k , Zeeman splitting of the energy bands makes a conventional CDW ground state energetically unfavourable [89], possibly yielding a novel modulated CDW state like that proposed for $(\text{Per})_2\text{Au}(\text{mnt})_2$ (see Section 2 and Refs. [82, 83]). In $-(\text{BEDT-TTF})_2\text{KHg}(\text{SCN})_4$ this state is es-

pecially unusual due to the existence of the 2D pocket, which appears to be ungapped by CDW formation [79]. The CDW and 2D hole pocket screen each other, with pinning of the CDW then enabling a non-equilibrium distribution of orbital magnetization throughout the bulk [79]. Consequently, such a state exhibits a critical state analogous to that in type II superconductors. Some of us have discussed this in more detail in another Chapter of this book.

1.7 Summary

We have tried to illustrate why some members of the high-field community are fond of charge-transfer salts. This enthusiasm is likely to continue for some time, as the charge-transfer salts offer great versatility as a playground for studying the formation of band structure. Using the known self-organisational properties of small organic molecules, one can really indulge in "molecular architecture", in which the structure of a charge-transfer salt is adjusted to optimise a desired property [25]. The most imaginative essays in this field involve the use of molecules that introduce a further property which modifies the electronic behaviour, such as chirality or the presence of magnetic ions [91]; in the latter case, one of the aims is to manufacture an organic Kondo system. Some recent experimental data from three such compounds are presented in Figure 1.13; the salts in question have the generic formula $-(\text{BEDT-TTF})_2 [\text{H}_3\text{OM}(\text{C}_2\text{O}_4)_3] (\text{Sol})$, where M is a transition ion, and Sol is an incorporated solvent molecule. The M ion allows one to introduce magnetic moments in a controllable way, whereas changing the solvent molecule allows the details of the unit cell structure to be altered [91]. As Figure 1.13 shows, such adjustments cause very distinct changes to the Fermi-surface topology, reflected in the magnetic quantum oscillation spectra [11,19]. Some of these salts appear to be superconductors.

There are also many reasons for continuing to study charge-transfer salts at high magnetic fields. A particular goal is the ultraquantum limit, in which only one quantised Landau-level is occupied; phenomena such as yet more varieties of field-induced superconductivity have been predicted to occur once such a condition is attained [3,14,19]. Furthermore, there are many open questions as to the role of chiral Fermi liquids in such fields [14]. Another area of considerable interest is the observation of magnetic breakdown. At fields above 50 T, the magnetic energy of the holes in the organic superconductors is starting to become a substantial fraction of their total energy, and one gradually starts to approach the famous Hofstadter "butterfly" limit [14].

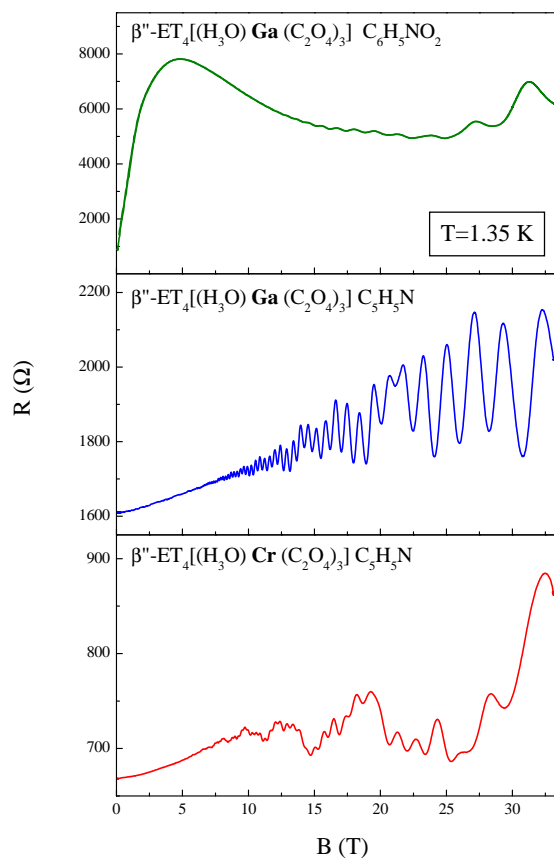


Fig. 1.13. Interlayer resistance of three different charge-transfer salts of the form $\beta''\text{-(BEDT-TTF)}_2[\text{H}_3\text{OM}(\text{C}_2\text{O}_4)_3](\text{Sol})$ (ET is an abbreviation of BEDT-TTF). The magnetic field is perpendicular to the highly-conducting planes. (after Reference [1, 19]).

Acknowledgements

This work is funded by US Department of Energy (DOE) grant LDRD 20040326ER. Work at NHMFL is performed under the auspices of the National Science Foundation, DOE and the State of Florida.

References

1. B.J. Powell and R.H. McKenzie, *J. Phys.: Condens. Matter* **16**, L367 (2004).
2. M.T. Dressel and N.D. Richko, *Chemical Reviews*, **104**, 5689 (2004).
3. J. Singleton and C.H. Mielke, *Contemp Phys.* **43**, 63 (2002).
4. B.J. Powell and R.H. McKenzie, *Phys. Rev. Lett.* **94**, 047004 (2005).
5. B.J. Powell and R.H. McKenzie, *Phys. Rev. B* **69**, 024519 (2004).
6. F. Kagawa, T. Itou, K. Miyagawa and K. Kanoda, *Phys. Rev. Lett.* **93**, 127001 (2004).
7. S. Lefebvre, P. Wzietek, S. Brown, C. Bourbonnais, D. Jormé, C. Mizere, M. Fournier, and P. Batail, *Phys. Rev. Lett.* **85**, 5420 (2000).
8. R.D. McDonald, A.K. Klehe, J. Singleton and W. Hayes, *J. Phys.: Condens. Matter* **15**, 5315 (2003).
9. P.A. Goddard, S.J. Blundell, J. Singleton, R.D. McDonald, A. Ardavan, A. Narduzzo, J.A. Schlueter, A.M. Kini, T. Sasaki, *Phys. Rev. B* **69**, 174509 (2004).
10. J. Singleton, C.H. Mielke, W. Hayes, J.A. Schlueter, *J. Phys.: Condens. Matter* **15**, L203 (2003).
11. A.I. Coldea, A.F. Bangura, J. Singleton, A. Ardavan, A. Akutsu-Sato, H. Akutsu, S.S. Tumer and S.P. Day *Phys. Rev. B* **69**, 085112 (2004).
12. J. Merino and R.H. McKenzie, *Phys. Rev. Lett.* **87**, 237002 (2001).
13. P.A. Goddard, S.W. Tozer, J. Singleton, A. Ardavan, A. Abate and M. Kummoo, *J. Phys.: Condens. Matter* **14**, 7345 (2002).
14. J. Singleton, *Rep. Prog. Phys.* **63**, 1111 (2000).
15. S. Uji, H. Shinagawa, T. Terashima, T. Yakabe, Y. Terai, M. Tokumoto, A. Kobayashi, H. Tanaka and H. Kobayashi, *Nature* **410**, 908 (2001).
16. J. Singleton, J.A. Symington, M.S. Nam, A. Ardavan, M. Kummoo and P. Day, *J. Phys.: Condens. Matter* **12**, L641 (2000).
17. V.F. Mitrovic, M. Horvatic, C. Bethier, G. Knebel, G. Lapertot, J. Fluquet, *Phys. Rev. Lett.*, in press (2006).
18. M.A. Tanatar, T. Ishiguro, H. Tanaka and H. Kobayashi, *Phys. Rev. B* **66**, 134503 (2002).
19. A.F. Bangura, A.I. Coldea, J. Singleton, A. Ardavan, A. Akutsu-Sato, T. Akutsu, S.S. Tumer, P. Day, T. Yamamoto and K. Yakushi, *Phys. Rev. B* **72**, 014543 (2005).
20. J. Schmalian, *Phys. Rev. Lett.* **81**, 4232 (1998).
21. J.M. Cauley, W. Lubczynski, F.L. Pratt, J. Singleton, D.Y.K. Ko, W. Hayes, M. Kummoo and P. Day, *J. Phys.: Condens. Matter* **6**, 2911 (1994).
22. J. Singleton, P.A. Goddard, A. Ardavan, N. Harrison, S.J. Blundell, J.A. Schlueter and A.M. Kini, *Phys. Rev. Lett.* **88**, 037001 (2002).
23. N.W. Ashcroft and N.D. Mermin, *Solid State Physics*, Saunders (1976).
24. *Band theory and electronic properties of solids*, J. Singleton (Oxford University Press, Oxford, 2001).
25. Mori has summarised the structural properties of virtually all organic superconductors in three excellent review articles: T. Mori, *Bull. Chem. Soc. Jpn.* **71**, 2509 (1998); T. Mori, H. Mori, S. Tanaka, *Bull. Chem. Soc. Jpn.* **72**, 179 (1999); T. Mori, *Bull. Chem. Soc. Jpn.* **72**, 2011 (1999).
26. *Organic Superconductors* by T. Ishiguro, K. Yamaji and G. Saito (Springer-Verlag, Berlin 1998).

27. M.V. Kartsovnik, V.N. Laukhin, S.I. Pesotskii, I.F. Schegolev, V.M. Yakovenko, *J. Phys. I (Paris)* 2, 89 (1990).
28. Fermi surfaces of low-dimensional organic metals and superconductors by J. Wosnitza (Springer-Verlag, Berlin 1996).
29. N. Harrison, E. Rzepniewski, J. Singleton, P.J. Gee, M.M. Honold, P. Day and M. Kummoo, *J. Phys.: Condens. Matter* 11, 7227 (1999).
30. D. Beckmann, S. Wanka, J. Wosnitza, J.A. Schlueter, J.M. Williams, P.G. Nixon, R.W. Winter, G.L. Gard, J. Ren and M.H. Whangbo, *Eur. Phys. J. B* 1, 295 (1998); J. Wosnitza, S. Wanka, J.S. Qualls, J.S. Brooks, C.H. Mielke, N. Harrison, J.A. Schlueter, J.M. Williams, P.G. Nixon, R.W. Winter and G.L. Gard, *Synth. Met.* 103, 2000 (1999); F. Zuo, X. Su, P. Zhang, J.S. Brooks, J. Wosnitza, J.A. Schlueter, J.M. Williams, P.G. Nixon, R.W. Winter, G.L. Gard, *Phys. Rev. B* 60, 6296 (1999); J. Wosnitza, *Physica B* 246-247, 104 (1998).
31. M. D'Amore, J. Singleton, F.L. Pratt, J. Caulfield, W. Hayes, J.A.A. Perenboom, I. Deckers, G. Pitsi, M. Kummoo and P. Day, *Phys. Rev. B*, 49, 3934 (1994).
32. A.A. House, N. Harrison, S.J. Blundell, I. Deckers, J. Singleton, F. Herlach, W. Hayes, J.A.A. Perenboom, M. Kummoo and P. Day, *Phys. Rev. B* 53, 9127 (1996).
33. C.H. Mielke, J. Singleton, M.-S. Nam, N. Harrison, C.C. Agosta, B. Fraveland L.K. Montgomery, preprint cond-mat/0103501, *J. Phys.: Condens. Matter*, 13, 8325 (2001).
34. E. Demiralp and W.A. Goddard III, *Phys. Rev. B*, 56, 11907 (1997).
35. J. Liu, J. Schmalian, N. Trivedi, *Phys. Rev. Lett.* 94, 127003 (2005).
36. H.O. Jeschke and G. Kotliar, *Phys. Rev. B* 71, 085103 (2005).
37. D.G. Clarke and S.P. Strong, *Adv. Phys.* 46, 545 (1997); *J. Phys.: Condens. Matter* 8, 5415 (1996).
38. L.B. Ioffe and A.J. Millis, *Science* 285, 1241 (2000).
39. C. Bergermann, S.R. Julian, A.P. Mackenzie, S. Nishizaki and Y. Maeno, *Phys. Rev. Lett.* 84, 2662 (2000).
40. C.N.R. Rao, *J. Mater. Chem.* 9, 1 (1999).
41. R.H. McKenzie and P. Moses, *Phys. Rev. Lett.* 81, 4492 (1998); *Phys. Rev. B* 60, 11241 (1999).
42. This is roughly equivalent to the Mott-Ioffe-Regel criterion [43]; see e.g. [41] or Section 7.2 of [37].
43. N.F. Mott and E.H. Davies *Electronic properties of non-crystalline materials* (Taylor and Francis, London, 1975); A.F. Ioffe and A.R. Regel, *Prog. Semicond.*, 4, 237 (1960).
44. See e.g. *The theory of superconductivity in the high T_c cuprates*, P.W. Anderson (Princeton University Press, 1997), page 50.
45. K. Kuroki and H. Aoki, *Phys. Rev. B* 60, 3060 (1999).
46. R. Louati, S. Char-Kaddour, A. Ben Ali, R. Bennaceau and M. Heritier, *Synth. Met.* 103, 1857 (1999).
47. M.-S. Nam, S.J. Blundell, A. Ardavan, J.A. Symington and J. Singleton, *J. Phys.: Condens. Matter* 13, 2271 (2001).
48. J.M. Schram, J. Singleton, R.S. Edwards, A. Ardavan, E. Rzepniewski, R. Harris, P. Goy, M. Gross, J. Schlueter, M. Kummoo and P. Day, *J. Phys.: Condens.* 13 2235 (2001)

49. J. Singleton, R.S. Edwards in *High Magnetic Fields, Science and Technology; Volume 2, Theory and Experiment*, eds. F. Herlach and N. Miura (World Scientific, Singapore 2003), p. 85.
50. P.A. Goddard, S.J. Blundell, J. Singleton, R.D. McDonald, A. Ardavan, A. Narduzzo, J.A. Schlueter, A.M. Kini, and T. Sasaki, *Phys. Rev. B* 69 174509 (2004).
51. J. Singleton, P.A. Goddard, A. Ardavan, S.J. Blundell, A. Coldea and J. Schlueter, *Phys. Rev. Lett.* submitted, (2006), arXiv:cond-mat/0610318.
52. The existence of such a modulation might suggest that a beating between "neck and belly" frequencies would be observed in the dHvA effect [14]; however, in careful low-field studies [53], no such beating has been observed. We shall see that this is because the typical cyclotron energy is rather greater than t_z , even at the lowest fields used.
53. T. Sasaki, W. Biberacher, K. Neumaier, W. Hehn, K. Andres and T. Fukase, *Phys. Rev. B* 57, 10889 (1998).
54. When viewed in the extended zone scheme, the quasi-two-dimensional section of this type of Fermi surface (blue in Fig. 1.3(c)) is often known as a "coke-bottle" Fermi surface (USA) or a "Cumberland sausage" Fermi surface (Europe). (The latter is a hand-made sausage with weak but approximately regular corrugations.)
55. This simple discussion deals with an interlayer transfer integral directed along the normal to the layers. However, most real charge-transfer salts have rather lower symmetry, and it is imperative that the correct direction of the interlayer transfer integral be taken into account; see Ref. [50].
56. T. Osada, S. Kagoshima and N. Miura, *Phys. Rev. Lett.* 77, 5261 (1996); N. Hanasaki, S. Kagoshima, T. Hasegawa, T. Oosada and N. Miura, *Phys. Rev. B* 57, 1336 (1998); *ibid.* 60, 11210 (1999)
57. V.G. Peschansky and M.V. Kartsovnik, *Phys. Rev. B* 60, 11207 (1999); I.J. Lee and M.J. Naughton, *Phys. Rev. B* 57, 7423 (1998).
58. E. Ohmichi, H. Ito, T. Ishiguro, T. Komatsu and G. Saito, *J. Phys. Soc. Jpn.* 66, 310 (1997)
59. V.M. Gvozdkov, J. Wosnitza, *Low Temperature Physics* 32, 109 (2006).
60. M.S. Nam, S.J. Blundell, A. Ardavan, J. Symington, J. Singleton, *J. Phys.: Condens. Matter* 13 2271 (2001)
61. S.J. Blundell and J. Singleton, *J. Physique I* 6, 1837 (1996).
62. N.E. Hussey, *J. Phys. Chem. Solids*, 67 227 (2006).
63. A. Bangura, A. Ardavan, S.J. Blundell, J. Singleton, P.A. Goddard, J. Schlueter, *Phys. Rev. Lett.*, submitted (2006).
64. N. Harrison, C.H. Mielke, J. Singleton, J.S. Brooks and M. Tokumoto, *J. Phys.: Condens. Matter* 13, L389 (2001).
65. C.C. Agosta, T. Coey, Z. Bayindir, I. Mhut, C. Martin, M. Tokumoto, *Int. J. Mod. Phys B* 30, 3227-32.
66. N. Harrison, R. Bogaerts, P. Reinders, J. Singleton, S.J. Blundell, F. Herlach, *Phys. Rev. B* 54 9977 (1996).
67. N. Harrison, J. Caulfield, J. Singleton, P.H.P. Reinders, F. Herlach, W. Hayes, M. Kumoo and P. Day, *J. Phys. Condens. Matter* 8, 5415 (1996).
68. A.E. Kovalev, T. Ishiguro, T. Kondo and G. Saito, *Phys. rev. B* 62, 103 (2000).
69. *Magnetic oscillations in metals* D. Shoenberg, (Cambridge University Press, 1984).

70. S. Hill, *Phys. Rev. B* **55**, 4931 (1997); *ibid.* **62**, 8699 (2000).
71. N. Harrison, J. Singleton, *J. Phys.: Condens. Matter*, **13**, L463 (2001).
72. Singleton, J., in *Encyclopedia of Condensed Matter Physics*, eds F. Bassani, G.L. Liedl and P. Wyder, vol. 1, p. 343 (Elsevier, Oxford, 2005).
73. J. Singleton, C.H.Mielke, W.Hayes and J.A.Schlueter *J. Phys.-Condens. Mat.*, **15** (12), L203-L211 (2003)
74. I.Mihut, C.C.Agosta, C.Martin, C.H.Mielke, T.Coey, M.Tokumoto, M.Kumoo, J.A.Schlueter, P.A.Goddard, N.Harrison, *Phys. Rev. B* **73** 125118 (2006).
75. M.Tinkham, *Introduction to Superconductivity* (McGraw-Hill, 1994).
76. G.Gruner, *Density waves in solids*, *Frontiers in physics* **89** (Addison-Wesley, 1996).
77. N.Harrison, L.Balicas, J.S.Brooks and M.Tokumoto, *Phys. Rev. B* **62**, 14212 (2000).
78. D.Andres, M.V.Kartsovnik, P.D.Grigoriev, W.Biberacher and H.Muller, *Phys. Rev. B* **68**, 201101 (2003).
79. N.Harrison, J. Singleton, A.Bangura, A.Ardavan, P.A.Goddard, R.D.McDonald and L.K.Montgomery, *Phys. Rev. B* **69**, 165103 (2004).
80. M.Matos, G.Bonfait, R.T.Henriques and M.AImeida, *Phys. Rev. B* **54**, 15307 (1996).
81. D.Graf, J.S.Brooks, E.S.Choi, S.Uji, J.C.Dias, M.AImeida and M.Matos, *Phys. Rev. B* **69**, 125113 (2004).
82. R.McDonald, N.Harrison, J. Singleton, A.Bangura, P.A.Goddard, A.P.Ramirez, X.Chi, *Phys. Rev. Lett.* **94**, 106404 (2005).
83. R.McDonald, N.Harrison, L.Balicas, K.H.Kim, J. Singleton and X.Chi, *Phys. Rev. Lett.* **93**, 076405 (2004).
84. R.D.McDonald, N.Harrison, P.Goddard, J. Singleton, X.Chi, *cond-mat* 0408408 (2004).
85. R.T.Henriques, *J. Phys. C* **17**, 5197 (1984).
86. D.Graf, E.S.Choi, J.S.Brooks, M.Matos, R.T.Henriques and M.AImeida, *Phys. Rev. Lett.* **93**, 076406 (2004).
87. A.G.Lebed, *JETP Letters* **78**, 138 (2003).
88. P.M.Chaikin, *J. Phys. I (France)* **6**, 1875 (1996).
89. R.H.McKenzie, *cond-mat*/970635.
90. R.D.McDonald, N.Harrison, *preprint* (2006).
91. Peter Day, *Phil. Trans. R. Soc. London* **357**, 3163 (1999).